Science Advances
AAAS

Supplementary Materials for

Synthetic genetic circuits to uncover the OCT4 trajectories of successful reprogramming of human fibroblasts

Katherine Ilia *et al*.

Corresponding author: Domitilla Del Vecchio, ddv@mit.edu;
Thorsten M. Schlaeger, thorsten.schlaeger@childrens.harvard.edu

Sci. Adv. **9**, eadg8495 (2023)
DOI: 10.1126/sciadv.adg8495

The PDF file includes:

Other Supplementary Material for this manuscript includes the following:

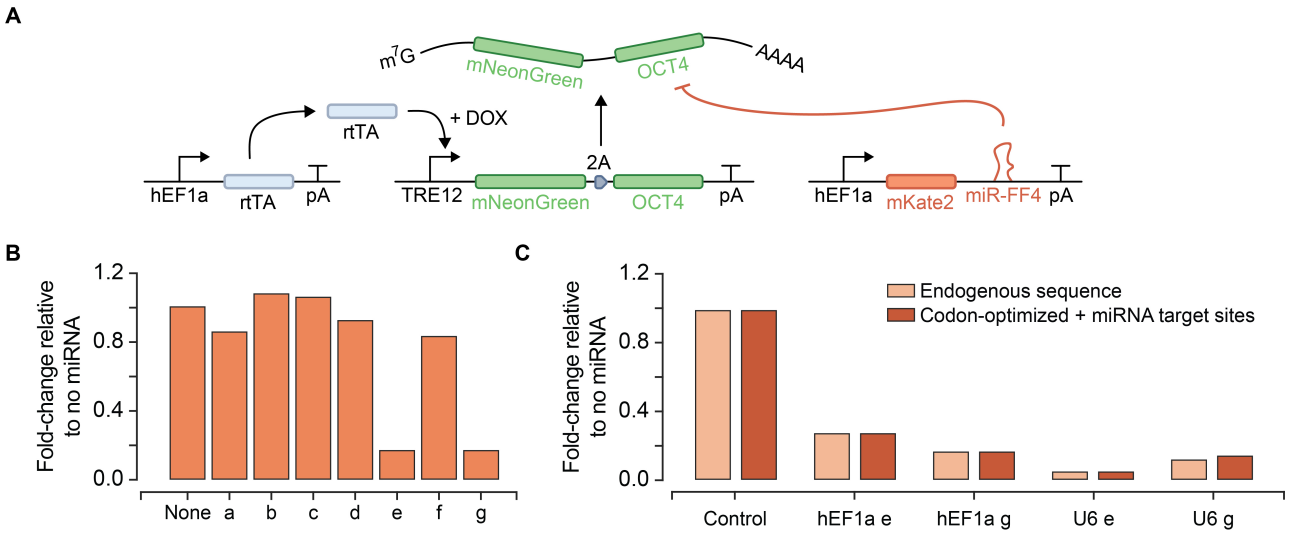

Fig. S1. Implementation of a strategy to overwrite Oct4 expression. **(A)** Schematic of the circuit used to assay the functional activity of miRNAs to knock down OCT4. The expression of OCT4 is driven by rtTA and is DOX-inducible. The miRNA is expressed from a 3'UTR intron in a hEF1a_mKate2 reporter plasmid; mKate2 fluorescence reports miRNA expression. The miRNAs target the coding sequence of OCT4, and knockdown of OCT4 leads to knockdown of mNeonGreen reporter levels. **(B)** The bar graph summarizes the fold-changes in the median levels of mNeonGreen-2A-OCT4 in response to addition of the miR-Oct4 variants. Only miR-Oct4e and miR-Oct4g have substantial activity. The sequences for all the tested miRs are summarized in table S1. **(C)** Comparison of the expression vectors for miR-Oct4e and -g. hEF1a e/g corresponds to the vector used in fig. S1A,B.

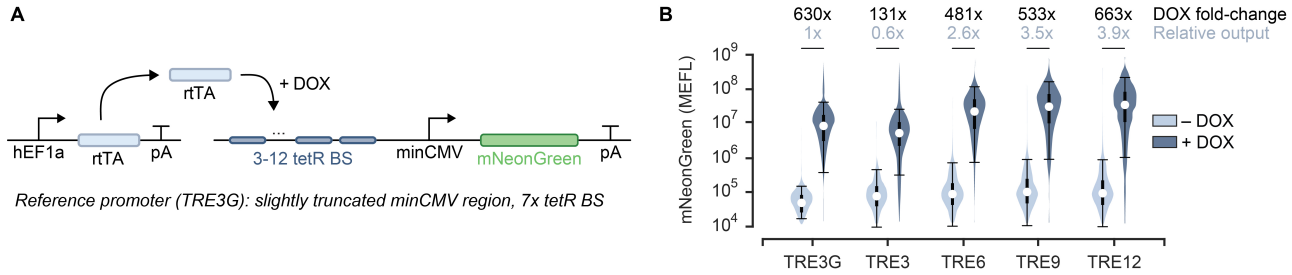

Fig. S2. Design and characterization of strong rtTA-activated promoters. **(A)** Schematic of the experimental design used to characterize strong rtTA-responsive promoters. We used rtTA as an activator and cloned different TRE promoters with 3–12 tetR binding sites upstream of a minimal CMV promoter to drive expression of an mNeonGreen reporter. **(B)** The violin plots summarize the mNeonGreen distribution in the absence and presence of DOX for each promoter variant. The inset box plots show the median (white circle), 25th to 75th percentiles (box), and 5th to 95th percentiles (error bars). The fold-changes written in black correspond to the ratio of the medians of the mNeonGreen output distributions in the presence and absence of DOX. The median mNeonGreen level in the on-state (+DOX) was normalized to that of the TRE3G promoter (values written in blue and labeled "relative output").

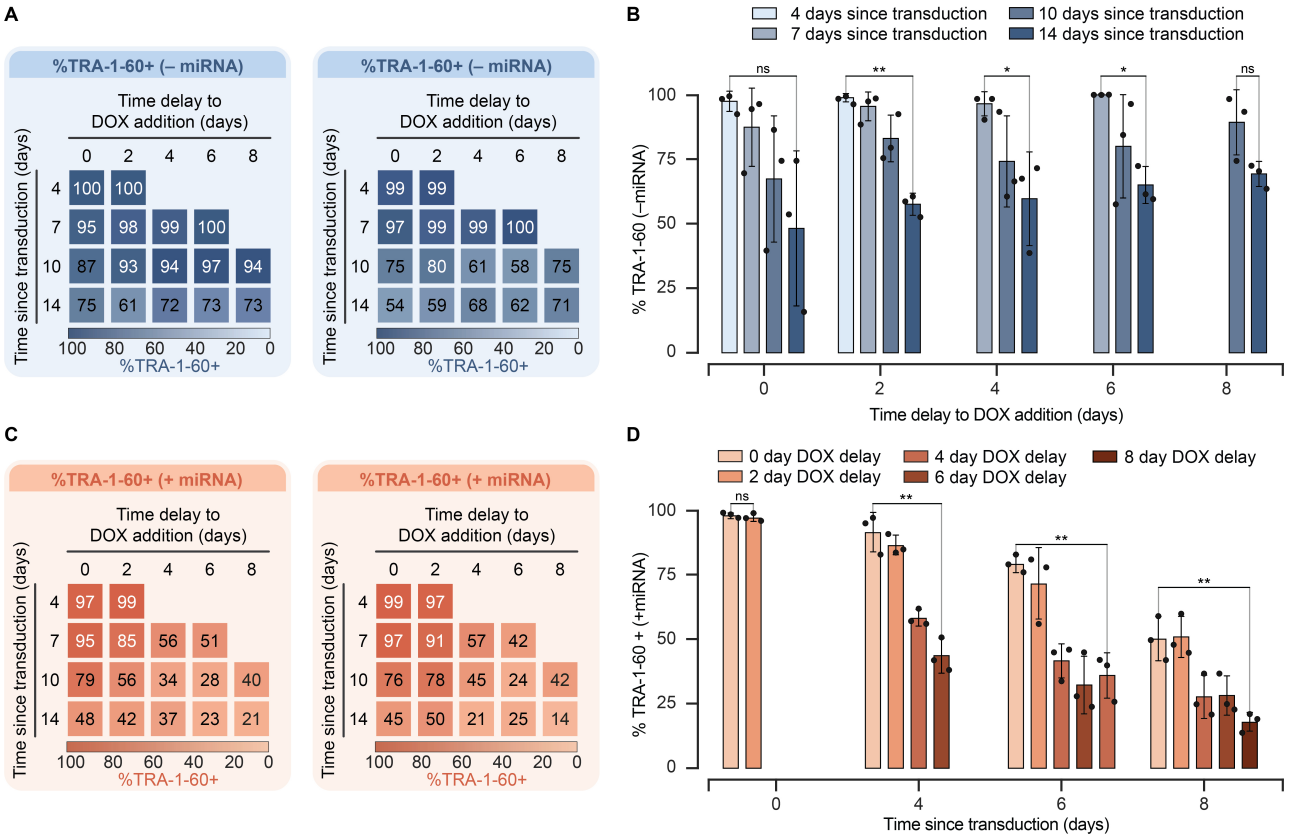

Fig. S3. The effect of overexpressing or knocking down OCT4 in hiPSCs. We transduced iPSCs with two versions of the two-lentivirus system shown in Fig. 2A, without **((A), (B))** and with **((C), (D))** U6-miR-Oct4e, and we cultured them in various doxycycline (DOX) conditions. "Time delay to DOX addition" refers to the number of days post-transduction when DOX was added to the medium. At every time since transduction, the heatmaps summarize the proportion of TRA-1-60-positive cells for each condition. The heatmaps in **(A)** and **(C)** represent replicates of the data in Fig. 2A. The heatmaps on the left and right summarize data from transduced 1157.2 cells and 1383.1 cells, respectively, while Fig. 2A summarizes data from transduced PGP-1 cells. In **(B)** and **(D)**, each bar represents the mean value of the proportion of TRA-1-60-positive cells for each condition. Error bars in the bar graph correspond to the standard deviations of n=3 biological replicates, each of which is plotted as a dot. Asterisks indicate significant differences (∗p<0.05, ∗∗p<0.01) according to an unpaired two-tailed Student's t test. ns: not significant.

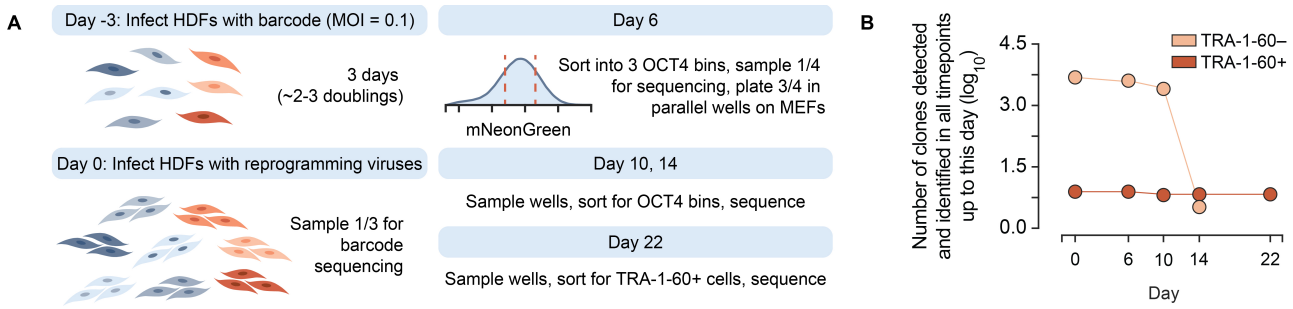

Fig. S4. Limitations of barcoding approaches for tracking OCT4 levels during human reprogramming. **(A)** Schematic overview of the barcoding experimental workflow. **(B)** The number of clones detected at each timepoint that were also detected at earlier timepoints decreases dramatically at later timepoints during reprogramming. In addition, the fact that reprogramming of human fibroblasts yields a low number of TRA-1-60-positive colonies represents a major bottleneck to tracking successful clones via a barcoding approach.

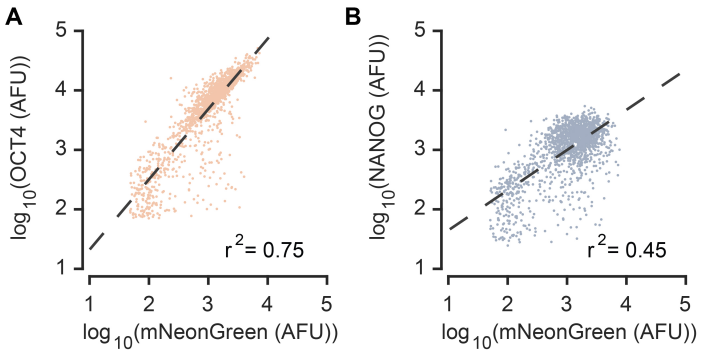

Fig. S5. Validation of the correlation between mNeonGreen and OCT4 from the imaging data. **(A)** For the stained colony in Fig. 4C, the correlation between the mNeonGreen and OCT4 fluorescence was determined. **(B)** As a negative control, the correlation between the mNeonGreen and NANOG (which is not expected to be correlated to mNeonGreen) fluorescence was also determined.

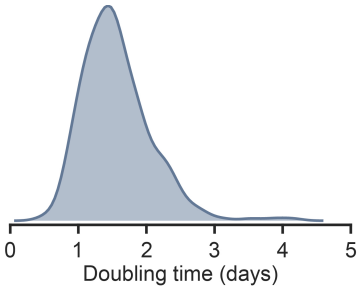

Fig. S6. Doubling time of successfully reprogramming HDFs. The distribution summarizes the estimated doubling time for every reconstructed trajectory over the duration of the entire timecourse. We found that these cells had a median doubling time of 1.83 days, which contrasts with studies of murine reprogramming, in which hyperproliferative cells have been shown to be more likely to successfully reprogram (59, 60).

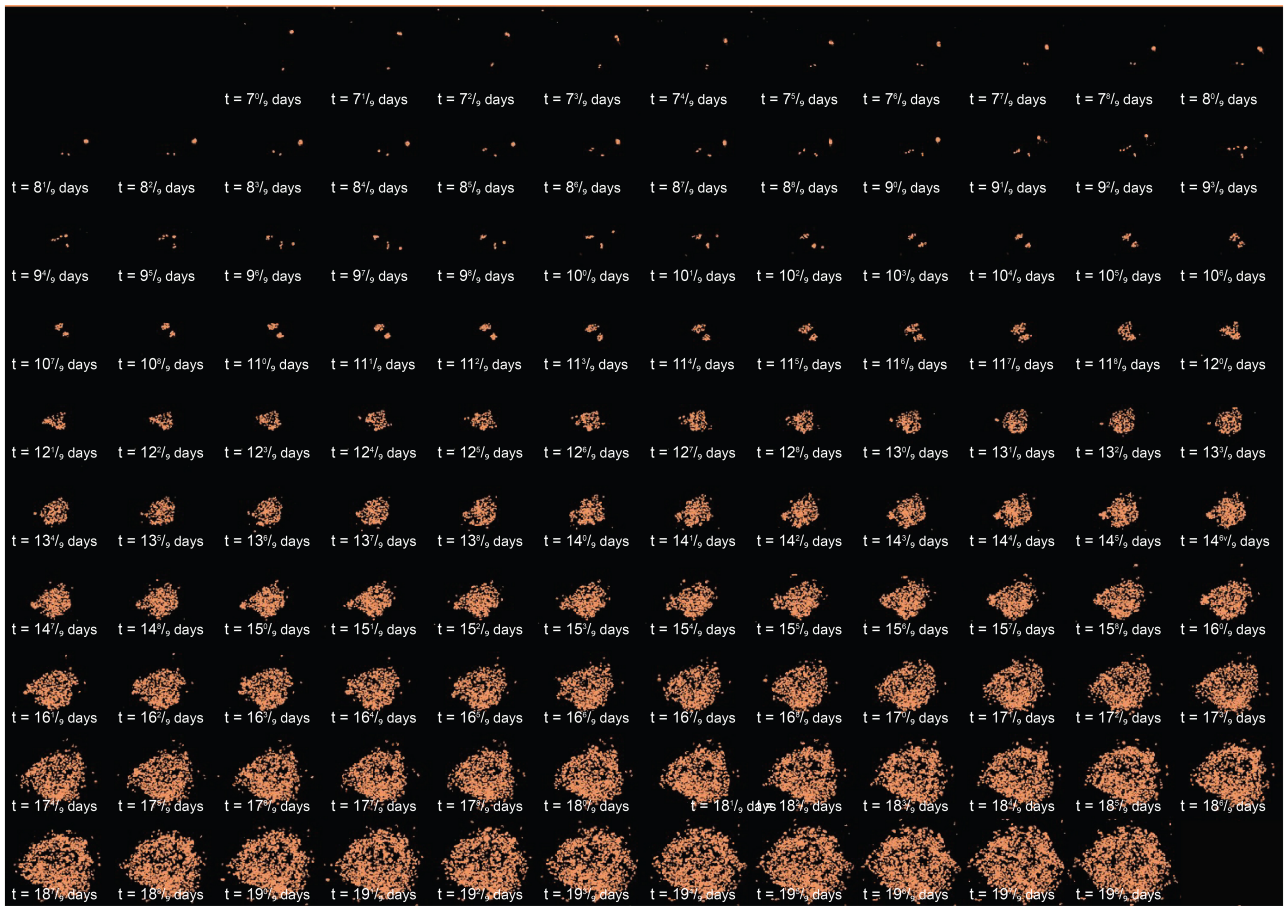

Fig. S7. Example of a colony formation event. We imaged the cells undergoing reprogramming 9 times a day. Each of the above images illustrates the state of an example colony formation event at the labeled timepoint.

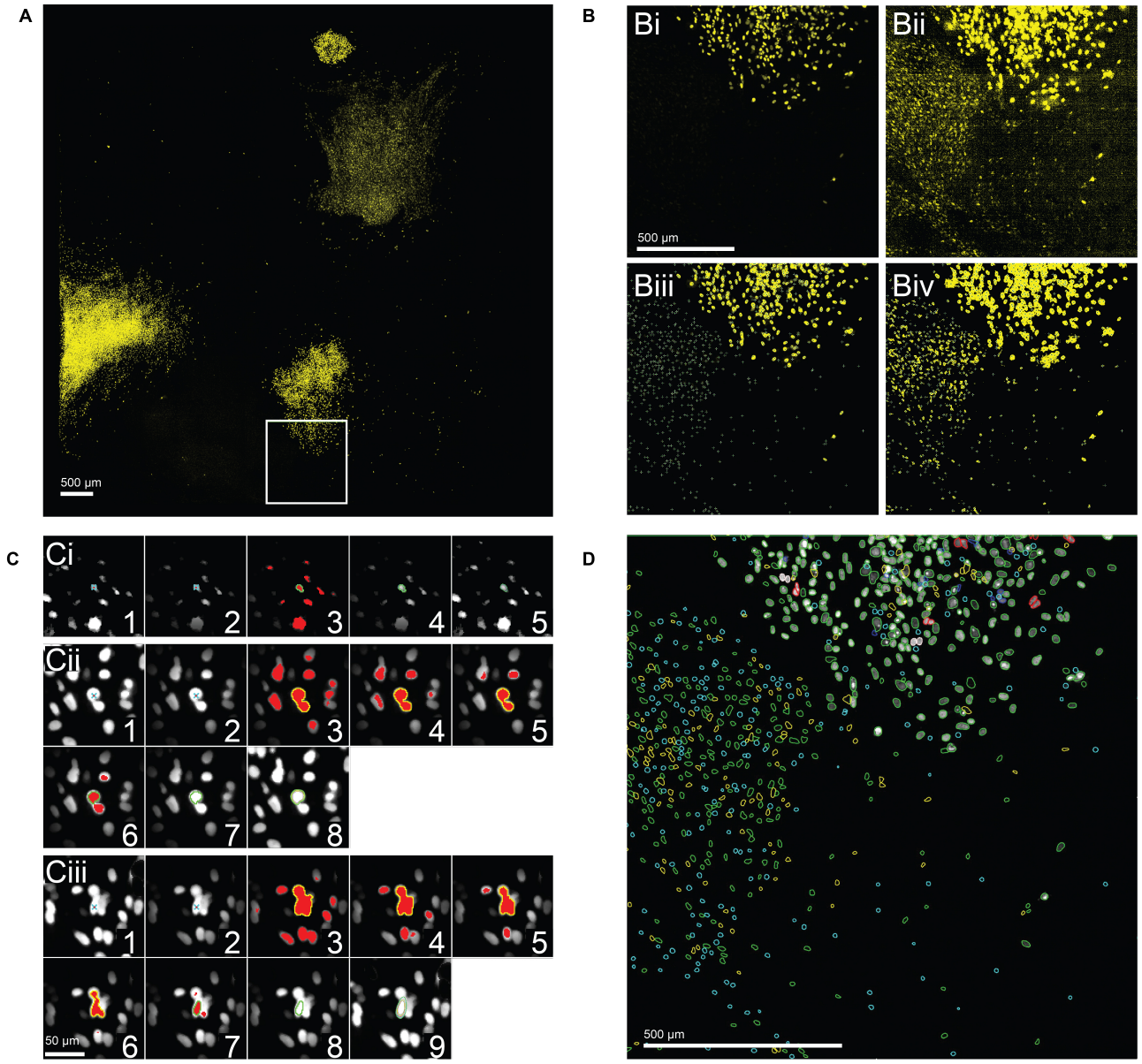
A
500 µm
B
Bi
Bii
Biii
Biv
500 µm
C
Ci
Cii
Ciii
50 µm
D
500 µm
E
log10(mNeonGreen (AFU))
y position (pixels)
F
Measured median InSpeck bead intensity (x 10^5)
Lot-adjusted InSpeck bead nominal intensity (%)
y = 10932x
r2 = 0.9996

Fig. S8. Identification, segmentation, and fluorescence intensity measurement of nuclei in confocal time-course imaging datasets. **(A)** The Z-projected "C13" live confocal image represents the ratio of the mNeonGreen (C01) and empty channel (C03) signals. The square indicates the region shown in panel (B). Scale bar: 500 µm. **(B)** Scale bar: 500 µm. **(Bi)** This image is a zoom-in version of the square in panel (A). **(Bii)** We enhanced the signal from the image in panel (Bi) 40x to visualize very dim cells. **(Biii)** After image processing (removal of bright outliers, despeckling, and image median subtraction), we identified the local maxima and marked them with crosshairs. **(Biv)** This image is the same as the one in panel (Biii), with a 40x increase in the image brightness to enhance the visibility of cells with low mNeonGreen signal intensity. **(C)** For each identified local maximum, the algorithm triggers a search for a nucleus-shaped and -sized region of interest (ROI). Scale bar: 50 µm. **(Ci)** The image sequence illustrates the identification of a dim cell. The first panel contains a 100x100 pixel cropped region with the candidate location in the center and the local maximum marked by a cyan cross with a red dot. This image is then progressively dimmed towards the periphery to suppress signal from nearby nuclei that may be brighter (panel 2). An intensity threshold is applied and repeatedly increased until the thresholded area (red) that contains the maximum area that passes the size- and shape-based inclusion gates (panel 3). Panel 4 shows the identified region without thresholding. The identified nuclear outline is then smoothened and isometically scaled to more accurately capture the identified nuclear ROI (panel 5). **(Cii)** The image sequence summarizes an example of the cell identification algorithm in a case where there is a bright nuclear region that is in contact with another nuclear region, requiring a higher threshold (panel 3-6). Panels 1-5 display the processing steps summarized in Ci. A more significant isometric enlargement is applied to this ROI to compensate for the smaller size of the initial ROI due to the higher threshold level (panel 8: the final ROI is outlined by a thick green line). **(Ciii)** The image sequence shows an example of the cell identification and segmentation algorithm in a case where there is a nuclear region that overlaps with multiple other nuclear regions. **(D)** The outlines represent all of the nuclear regions identified in the images in panel (B). The nuclear regions are outlined in colors that indicate in which step of the multi-step nuclear ROI identification process they were accepted. Step 1 (green) involves dynamic thresholding; Step 2 (yellow) involves an attempt of maxima-based de-clumping followed by dynamic thresholding; Step 3 (cyan) involves accepting ROIs based on area thresholds alone using a single minimal threshold setting of 1 to capture very dim cells. After an ROI is accepted, the signal contained within it is removed. Finally, Step 4 (cyan) involves identification of additional local maxima and nuclei after completion of Steps 1-3. We also leveraged additional algorithms to aid the segmentation of overlapping nuclei, including ROI splitting (red) and binary ROI watershedding (pink). All steps were performed using macros in FIJI/ImageJ. Scale bar: 500 µm. **(E)** Each point represents the measured C13 integrated fluorescence intensity over the Y location of the nuclei from the same well and timepoint shown in panel (A), demonstrating that the described multistep ROI ID approach enables the robust detection and segmentation of nuclei with mNeonGreen expression levels span over three orders of magnitude. **(F)** We plated InSpeck fluorescent beads with nominal FITC fluorescence intensity levels of 1%, 10%, and 30% into wells and imaged using the same settings described in the Methods. Each point in the plot represents the integrated CO1 (mNeonGreen) intensity level of the beads against the lot-corrected nominal bead intensities. We employed beads from the same lot in flow cytometry experiments to facilitate a direct comparison of mNeonGreen fluorescence intensities between flow cytometry and confocal imaging experiments.

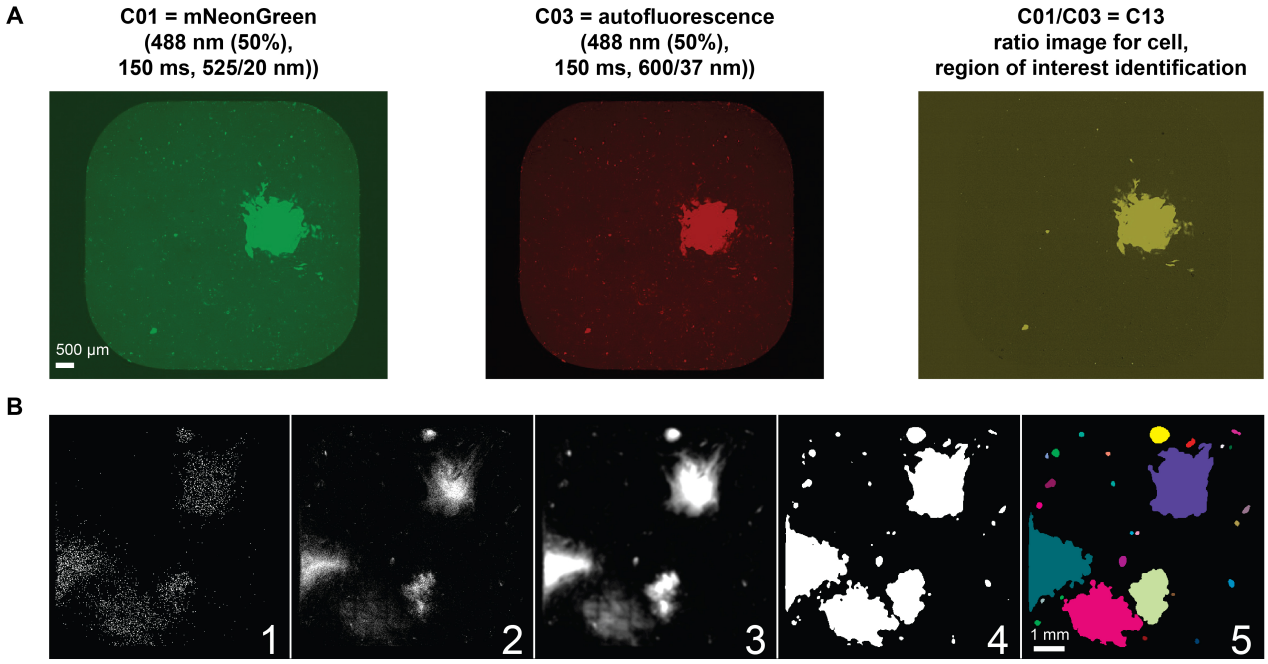

Fig. S9. Image processing methodology. (A) To facilitate image alignment throughout the timecourse and identification of regions of interest, we calculated a ratio image ("C13") by dividing the signal intensity from the pre-processed mNeonGreen ("C01") and autofluorescence ("C03") channel images. Scale bar: 500 µm. **(B)** We identified the colony regions by drawing a white circle at the location of each identified cell (panel 1 shows this for an example well) followed by summation of the timepoint slices (panel 2), blurring (panel 3), thresholding (panel 4), and size selection and filling of holes (panel 5). Scale bar: 1 mm.

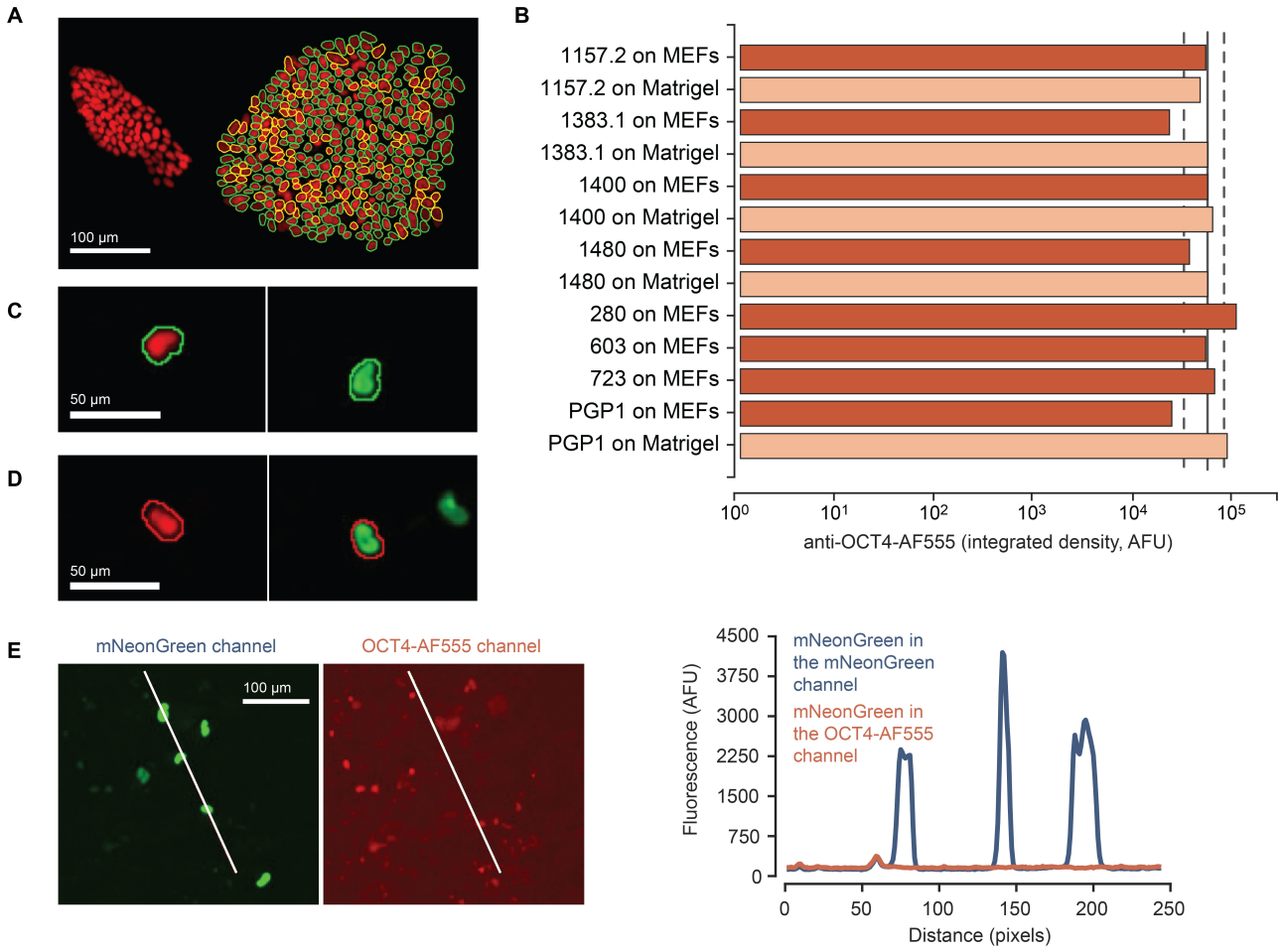

Fig. S10. Quantification of OCT4, SOX2, and OCT4-mNeonGreen expression levels in hiPSCs and transduced HDFs. (A) Immunofluorescence of anti-OCT4-AF555 staining facilitates identification of nuclear ROIs for an undifferentiated iPSC colony (line 1480). Scale bar: 100 µm. **(B)** To estimate the OCT4 expression levels in undifferentiated iPSCs, we plated several different lines on MEFs or Matrigel and stained for OCT4. Each bar represents the mean of the OCT4 expression level (equivalent to the mean of the integrated fluorescence intensities of all nuclei in a colony) in each colony for at least three colonies per condition. The solid gray line and the dashed gray lines represent the geometric mean and standard deviation, respectively. We compiled these data from 79 undifferentiated colonies from 8 hiPSC lines and three independent experiments. **(C)** To determine the ratio of OCT4 immunofluorescence and mNeonGreen fluorescence signal for the OCT4-mNeonGreen fusion protein, we infected HDFs with our controllers, stained for OCT4 seven days post-transduction, and imaged for mNeonGreen and anti-OCT4-AF555. The images give an example of an ROI of a transduced and OCT4-stained HDF nucleus and the accepted ROI of the successfully identified nucleus of the same cell during live imaging for mNeonGreen. Scale bar: 50 µm. **(D)** For the same assay as in panel (C), these images give an example of a cell rejected by the identification algorithm because of the presence of two nearby candidate nuclei in the mNeonGreen image, thus precluding unambiguous identification of the correct mNeonGreen-positive nucleus. Scale bar: 50 µm. **(E)** There is an absence of signal in the OCT4 (Alexa Fluor 555) channel in images of the transduced cells. We acquired these confocal images post-fixation and pre-immunostaining. The profile plots show per-pixel intensities under the diagonal white line in the images. Scale bar: 100 µm.

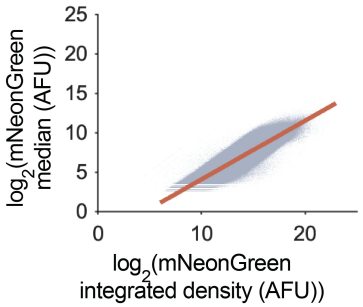

Fig. S11. There is a strong correlation between the median mNeonGreen intensity and the integrated density of the mNeonGreen signal for cells identified in the imaging data. For each cell at every timepoint, we plotted the integrated density and the median of all the pixels within the nuclear ROI. The orange line represents the linear regression of the points, with $r^2 = 0.91$.

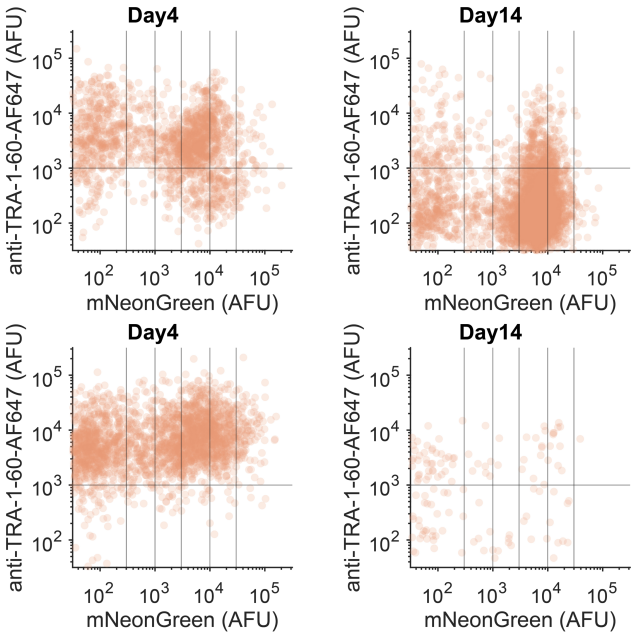

Fig. S12. The effects of ectopic OCT4 expression on pluripotency. We transduced iPSCs with the version of the system shown in Fig. 2A containing the miRNA cassette and maintained them in DOX-containing medium. We stained the cells for TRA-1-60 four and fourteen days post-transduction and analyzed them via flow cytometry. The above scatter plots correspond to the replicates of the data in Fig. 2B.

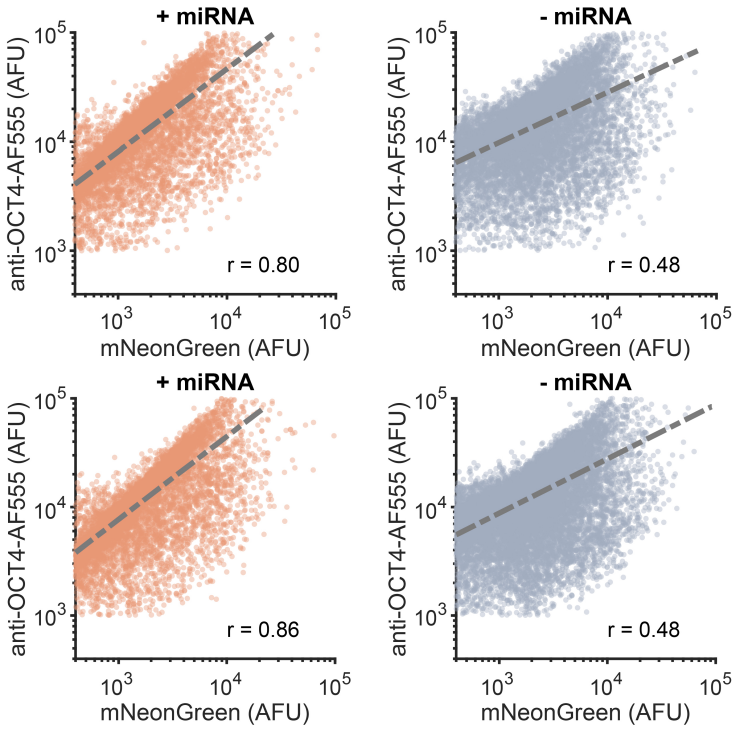

Fig. S13. mNeonGreen and total OCT4 are correlated in iPSCs transduced with the trajectory generator. We transduced iPCSs with the two illustrated two-lentivirus systems. We stained the transduced cells for OCT4 four days post-transduction and analyzed them via flow cytometry. The scatter plots show the double-positive (OCT4, mNeonGreen) cells. The dashed lines represent the linear regression fit of these points, with the corresponding r-value shown in the respective plot. The above scatter plots correspond to the replicates of the data in Fig. 3D.

Name	Sequence
miR-Oct4a	AGGATGTGGTCCGAGTGTGGT
miR-Oct4b	AACATGTGTAAGCTGCGGCCC
miR-Oct4c	GCCCTCACTTCACTGCACTGC
miR-Oct4d	TCTCCCATGCATTCAAACTGA
miR-Oct4e	GTGGAGGAAGCTGACAACAAT
miR-Oct4f	ATCTTCAGGAGATATGCAAAG
miR-Oct4g	GGTTCTATTTGGGAAGGTATT
miR-Oct4o	TTGGGATTAAGTTCTTCATTC

Table S1. miR-Oct4 variant sequences.

Primer	Sequence	Reference
OCT4 [FWD]	CCCCAGGGCCCCATTTTGGTACC	Tanabe *et al* (39)
OCT4 [REV]	ACCTCAGTTTGAATGCATGGGAGAGC	Tanabe *et al* (39)
SOX2 [FWD]	TGGCGAACCATCTCTGTGGT	Zapata-Linares et al (103)
SOX2 [REV]	CCAACGGTGTCAACCTGCAT	Zapata-Linares et al (103)
GAPDH [FWD]	ACGACCACTTTGTCAAGCTCATTTC	Swaidan *et al* (104)
GAPDH [REV]	GCAGTGAGGGTCTCTCTCTTCCTCT	Swaidan *et al* (104)

Table S2. RT-qPCR sequences.

Movie S1.

Timecourse imaging of reprogramming HDFs.

Data S1.

Tables including the experimental values for each main figure subpanel in which there are fewer that n = 20 points.

REFERENCES AND NOTES

1. K. Takahashi, S. Yamanaka, Induction of pluripotent stem cells from mouse embryonic and adult fibroblast cultures by defined factors. *Cell* **126**, 663–676 (2006).

2. K. Takahashi, K. Tanabe, M. Ohnuki, M. Narita, T. Ichisaka, K. Tomoda, S. Yamanaka, Induction of pluripotent stem cells from adult human fibroblasts by defined factors. *Cell* **131**, 861–872 (2007).

3. A. E. Omole, A. O. J. Fakoya, Ten years of progress and promise of induced pluripotent stem cells: Historical origins, characteristics, mechanisms, limitations, and potential applications. *PeerJ* **2018**, e4370 (2018).

4. Y. Y. Lipsitz, N. E. Timmins, P. W. Zandstra, Quality cell therapy manufacturing by design. *Nat. Biotechnol.* **34**, 393–400 (2016).

5. Y. Y. Lipsitz, P. Bedford, A. H. Davies, N. E. Timmins, P. W. Zandstra, Achieving efficient manufacturing and quality assurance through synthetic cell therapy design. *Cell* **20**, 13–17 (2017).

6. K. Takahashi, S. Yamanaka, A decade of transcription factor-mediated reprogramming to pluripotency. *Nat. Rev. Mol. Cell Biol.* **17**, 183–193 (2016).

7. T. M. Schlaeger, L. Daheron, T. R. Brickler, S. Entwisle, K. Chan, A. Cianci, A. DeVine, A. Ettenger, K. Fitzgerald, M. Godfrey, D. Gupta, J. McPherson, P. Malwadkar, M. Gupta, B. Bell, A. Doi, N. Jung, X. Li, M. S. Lynes, E. Brookes, A. B. Cherry, D. Demirbas, A. M. Tsankov, L. I. Zon, L. L. Rubin, A. P. Feinberg, A. Meissner, C. A. Cowan, G. Q. Daley, A comparison of non-integrating reprogramming methods. *Nat. Biotechnol.* **33**, 58–63 (2015).

8. Y. Buganim, D. A. Faddah, R. Jaenisch, Mechanisms and models of somatic cell reprogramming. *Nat. Rev. Genet.* **14**, 427–439 (2013).

9. K. Hochedlinger, R. Jaenisch, Induced pluripotency and epigenetic reprogramming. *Cold Spring Harb. Perspect. Biol.* **7**, a019448 (2015).

10. A. H. Lang, H. Li, J. J. Collins, P. Mehta, Epigenetic landscapes explain partially reprogrammed cells and identify key reprogramming genes. *PLOS Comput. Biol.* **10**, e1003734 (2014).

11. E. M. Chan, S. Ratanasirintrawoot, I. H. Park, P. D. Manos, Y. H. Loh, H. Huo, J. D. Miller, O. Hartung, J. Rho, T. A. Ince, G. Q. Daley, T. M. Schlaeger, Live cell imaging distinguishes bona fide human iPS cells from partially reprogrammed cells. *Nat. Biotechnol.* **27**, 1033–1037 (2009).

12. T. S. Mikkelsen, J. Hanna, X. Zhang, M. Ku, M. Wernig, P. Schorderet, B. E. Bernstein, R. Jaenisch, E. S. Lander, A. Meissner, Dissecting direct reprogramming through integrative genomic analysis. *Nature* **454**, 49–55 (2008).

13. J. S. Kim, H. W. Choi, S. Choi, H. G. Seo, S. H. Moon, H. M. Chung, J. T. Do, Conversion of partially reprogrammed cells to fully pluripotent stem cells is associated with further activation of stem cell maintenance- and gamete generation-related genes. *Stem Cells Dev.* **23**, 2637–2648 (2014).

14. S. M. Hussein, M. C. Puri, P. D. Tonge, M. Benevento, A. J. Corso, J. L. Clancy, R. Mosbergen, M. Li, D. S. Lee, N. Cloonan, D. L. Wood, J. Munoz, R. Middleton, O. Korn, H. R. Patel, C. A. White, J. Y. Shin, M. E. Gauthier, K. A. L. Cao, J. I. Kim, J. C. Mar, N. Shakiba, W. Ritchie, J. E. Rasko, S. M. Grimmond, P. W. Zandstra, C. A. Wells, T. Preiss, J. S. Seo, A. J. Heck, I. M. Rogers, A. Nagy, Genome-wide characterization of the routes to pluripotency. *Nature* **516**, 198–206 (2014).

15. S. Sebban, Y. Buganim, Nuclear reprogramming by defined factors: Quantity versus quality. *Trends Cell Biol.* **26**, 65–75 (2016).

16. L. A. Boyer, I. L. Tong, M. F. Cole, S. E. Johnstone, S. S. Levine, J. P. Zucker, M. G. Guenther, R. M. Kumar, H. L. Murray, R. G. Jenner, D. K. Gifford, D. A. Melton, R. Jaenisch, R. A. Young, Core transcriptional regulatory circuitry in human embryonic stem cells. *Cell* **122**, 947–956 (2005).

17. A. Radzisheuskaya, J. C. Silva, Do all roads lead to Oct4? The emerging concepts of induced pluripotency. *Trends Cell Biol.* **24**, 275–284 (2014).

18. G. Shi, Y. Jin, Role of Oct4 in maintaining and regaining stem cell pluripotency. *Stem Cell Res. Ther.* **1**, 1–9 (2010).

19. E. P. Papapetrou, M. J. Tomishima, S. M. Chambers, Y. Mica, E. Reed, J. Menon, V. Tabar, Q. Mo, L. Studer, M. Sadelain, Stoichiometric and temporal requirements of Oct4, Sox2, Klf4, and c-Myc

expression for efficient human iPSC induction and differentiation. *Proc. Natl. Acad. Sci. U.S.A.* **106**, 12759–12764 (2009).

20. A. Radzisheuskaya, G. Le Bin Chia, R. L. Dos Santos, T. W. Theunissen, L. F. C. Castro, J. Nichols, J. C. Silva, A defined Oct4 level governs cell state transitions of pluripotency entry and differentiation into all embryonic lineages. *Nat. Cell Biol.* **15**, 579–590 (2013).

21. F. Hammachi, G. M. Morrison, A. A. Sharov, A. Livigni, S. Narayan, E. P. Papapetrou, J. O'Malley, K. Kaji, M. S. Ko, M. Ptashne, J. M. Brickman, Transcriptional activation by oct4 is sufficient for the maintenance and induction of pluripotency. *Cell Rep.* **1**, 99–109 (2012).

22. S. Velychko, K. Adachi, K. P. Kim, Y. Hou, C. M. MacCarthy, G. Wu, H. R. Schöler, Excluding Oct4 from Yamanaka cocktail unleashes the developmental potential of iPSCs. *Cell Stem Cell* **25**, 737–753.e4 (2019).

23. G. Wu, D. Han, Y. Gong, V. Sebastiano, L. Gentile, N. Singhal, K. Adachi, G. Fischedick, C. Ortmeier, M. Sinn, M. Radstaak, A. Tomilin, H. R. Schöler, Establishment of totipotency does not depend on Oct4A. *Nat. Cell Biol.* **15**, 1089–1097 (2013).

24. D. C. Hay, L. Sutherland, J. Clark, T. Burdon, Oct-4 knockdown induces similar patterns of endoderm and trophoblast differentiation markers in human and mouse embryonic stem cells. *Stem Cells* **22**, 225–235 (2004).

25. H. Niwa, J.-I. Miyazaki, A. G. Smith, Quantitative expression of Oct-3/4 defines differentiation, dedifferentiation or self-renewal of ES cells. *Nat. Genet.* **24**, 372–376 (2000).

26. J. L. Kopp, B. D. Ormsbee, M. Desler, A. Rizzino, Small increases in the level of Sox2 trigger the differentiation of mouse embryonic stem cells. *Stem Cells* **26**, 903–911 (2008).

27. B. W. Carey, S. Markoulaki, J. H. Hanna, D. A. Faddah, Y. Buganim, J. Kim, K. Ganz, E. J. Steine, J. P. Cassady, M. P. Creyghton, G. G. Welstead, Q. Gao, R. Jaenisch, Reprogramming factor stoichiometry influences the epigenetic state and biological properties of induced pluripotent stem cells. *Cell Stem Cell* **9**, 588–598 (2011).

28. G. Nagamatsu, S. Saito, T. Kosaka, K. Takubo, T. Kinoshita, M. Oya, K. Horimoto, T. Suda, Optimal ratio of transcription factors for somatic cell reprogramming. *J. Biol. Chem.* **287**, 36273–36282 (2012).

29. D. Sui, Z. Sun, C. Xu, Y. Wu, M. R. Capecchi, S. Wu, N. Li, Fine-tuning of iPSC derivation by an inducible reprogramming system at the protein level. *Stem Cell Rep.* **2**, 721–733 (2014).

30. U. Tiemann, M. Sgodda, E. Warlich, M. Ballmaier, H. R. Schöler, A. Schambach, T. Cantz, Optimal reprogramming factor stoichiometry increases colony numbers and affects molecular characteristics of murine induced pluripotent stem cells. *Cytometry A* **79**, 426–435 (2011).

31. T. Brambrink, R. Foreman, G. G. Welstead, C. J. Lengner, M. Wernig, H. Suh, R. Jaenisch, Sequential expression of pluripotency markers during direct reprogramming of mouse somatic cells. *Cell Stem Cell* **2**, 151–159 (2008).

32. P. D. Tonge, A. J. Corso, C. Monetti, S. M. Hussein, M. C. Puri, I. P. Michael, M. Li, D. S. Lee, J. C. Mar, N. Cloonan, D. L. Wood, M. E. Gauthier, O. Korn, J. L. Clancy, T. Preiss, S. M. Grimmond, J. Y. Shin, J. S. Seo, C. A. Wells, I. M. Rogers, A. Nagy, Divergent reprogramming routes lead to alternative stem-cell states, *Nature* **516**, 192–197 (2014).

33. M. Francesconi, B. Di Stefano, C. Berenguer, L. de André-Aguayo, M. Plana-Carmona, M. Mendez-Lago, A. Guillaumet-Adkins, G. Rodriguez-Esteban, M. Gut, I. G. Gut, H. Heyn, B. Lehner, T. Graf, Single cell RNA-seq identifies the origins of heterogeneity in efficient cell transdifferentiation and reprogramming. *eLife* **8**, e41627 (2019).

34. K. A. Tran, S. J. Pietrzak, N. Z. Zaidan, A. F. Siahpirani, S. G. McCalla, A. S. Zhou, G. Iyer, S. Roy, R. Sridharan, Defining reprogramming checkpoints from single-cell analyses of induced pluripotency. *Cell Rep.* **27**, 1726–1741.e5 (2019).

35. V. Malik, L. V. Glaser, D. Zimmer, S. Velychko, M. Weng, M. Holzner, M. Arend, Y. Chen, Y. Srivastava, V. Veerapandian, Z. Shah, M. A. Esteban, H. Wang, J. Chen, H. R. Schöler, A. P. Hutchins, S. H. Meijsing, S. Pott, R. Jauch, Pluripotency reprogramming by competent and incompetent POU factors uncovers temporal dependency for Oct4 and Sox2. *Nat. Commun.* **10**, 3477 (2019).

36. G. Schiebinger, J. Shu, M. Tabaka, B. Cleary, V. Subramanian, A. Solomon, J. Gould, S. Liu, S. Lin, P. Berube, L. Lee, J. Chen, J. Brumbaugh, P. Rigollet, K. Hochedlinger, R. Jaenisch, A. Regev, E. S. Lander, Optimal-transport analysis of single-cell gene expression identifies developmental trajectories in reprogramming. *Cell* **176**, 928–943.e22 (2019).

37. E. Lujan, E. R. Zunder, Y. H. Ng, I. N. Goronzy, G. P. Nolan, M. Wernig, Early reprogramming regulators identified by prospective isolation and mass cytometry. *Nature* **521**, 352–356 (2015).

38. J. Elbaz, M. C. Puri, M. Faiz, K. W. Bang, L. Nguyen, B. Makovoz, M. Gertsenstein, S. M. Hussein, P. W. Zandstra, L. Briollais, N. Shakiba, A. Nagy, Highly efficient reprogrammable mouse lines with integrated reporters to track the route to pluripotency. *Proc. Natl. Acad. Sci. U.S.A.* **119**, e2207824119 (2022).

39. K. Tanabe, M. Nakamura, M. Narita, K. Takahashi, S. Yamanaka, Maturation, not initiation, is the major roadblock during reprogramming toward pluripotency from human fibroblasts. *Proc. Natl. Acad. Sci. U.S.A.* **110**, 12172–12179 (2013).

40. E. R. Zunder, E. Lujan, Y. Goltsev, M. Wernig, G. P. Nolan, A continuous molecular roadmap to iPSC reprogramming through progression analysis of single-cell mass cytometry. *Cell Stem Cell* **16**, 323–337 (2015).

41. M. Stadtfeld, N. Maherali, D. T. Breault, K. Hochedlinger, Defining molecular cornerstones during fibroblast to ips cell reprogramming in mouse. *Cell Stem Cell* **2**, 230–240 (2008).

42. Y. Buganim, D. A. Faddah, A. W. Cheng, E. Itskovich, S. Markoulaki, K. Ganz, S. L. Klemm, A. V. Oudenaarden, R. Jaenisch, Single-cell expression analyses during cellular reprogramming reveal an early stochastic and a late hierarchic phase. *Cell* **150**, 1209–1222 (2012).

43. L. V. Greder, S. Gupta, S. Li, M. J. Abedin, A. Sajini, Y. Segal, J. M. Slack, J. R. Dutton, Brief report: Analysis of endogenous Oct4 activation during induced pluripotent stem cell reprogramming using an inducible Oct4 lineage label. *Stem Cells* **30**, 2596–2601 (2012).

44. K.-P. Kim, Y. Wu, J. Yoon, K. Adachi, G. Wu, S. Velychko, C. M. MacCarthy, B. Shin, A. Röpke, M. J. Arauzo- Bravo, M. Stehling, D. W. Han, Y. Gao, J. Kim, S. Gao, H. R. Schöler, Reprogramming competence of OCT factors is determined by transactivation domains. *Sci. Adv.* **6**, eaaz7364 (2020).

45. C. Vogel, E. M. Marcotte, Insights into the regulation of protein abundance from proteomic and transcriptomic analyses. *Nat. Rev. Genet.* **13**, 227–232 (2012).

46. D. Del Vecchio, R. M. Murray, *Biomolecular Feedback Systems* (Princeton Univ. Press, 2015).

47. D. Del Vecchio, H. Abdallah, Y. Qian, J. J. Collins, A blueprint for a synthetic genetic feedback controller to reprogram cell fate. *Cell Systems* **4**, 109–120.e11 (2017).

48. X. Bofill-De Ros, S. Gu, Guidelines for the optimal design of miRNA-based shRNAs. *Methods* **103**, 157–166 (2016).

49. R. T. Rodriguez, J. M. Velkey, C. Lutzko, R. Seerke, D. B. Kohn, K. S. O'Shea, M. T. Firpo, Manipulation of OCT4 levels in human embryonic stem cells results in induction of differential cell types. *Exp. Biol. Med.* **232**, 1368–1380 (2007).

50. A. L. Szymczak, C. J. Workman, Y. Wang, K. M. Vignali, S. Dilioglou, E. F. Vanin, D. A. Vignali, Correction of multi-gene deficiency in vivo using a single 'self-cleaving' 2A peptide-based retroviral vector. *Nat. Biotechnol.* **22**, 589–594 (2004).

51. M. Q. Liu, M. Zhao, W. H. Kong, J. S. Peng, F. Wang, H. Y. Qiu, Z. R. Zhu, L. Tang, M. Sang, J. G. Wu, W. Z. Ho, W. Zhou, Antiretroviral therapy fails to restore levels of HIV-1 restriction miRNAs in PBMCs of HIV-1-infected MSM. *Medicine* **94**, e2116 (2015).

52. N. Plachta, T. Bollenbach, S. Pease, S. E. Fraser, P. Pantazis, Oct4 kinetics predict cell lineage patterning in the early mammalian embryo. *Nat. Cell Biol.* **13**, 117–123 (2011).

53. C. J. Lengner, F. D. Camargo, K. Hochedlinger, G. G. Welstead, S. Zaidi, S. Gokhale, H. R. Scholer, A. Tomilin, R. Jaenisch, Oct4 expression is not required for mouse somatic stem cell self-renewal. *Cell Stem Cell* **1**, 403–415 (2007).

54. A. Raj, C. S. Peskin, D. Tranchina, D. Y. Vargas, S. Tyagi, Stochastic mRNA synthesis in mammalian cells. *PLOS Biol.* **4**, 1707–1719 (2006).

55. A. Ochab-Marcinek, M. Tabaka, Bimodal gene expression in noncooperative regulatory systems. *Proc. Natl. Acad. Sci. U.S.A.* **107**, 22096–22101 (2010).

56. M. B. Elowitz, A. J. Levine, E. D. Siggia, P. S. Swain, Stochastic gene expression in a single cell. *Science* **297**, 1183–1186 (2002).

57. R. D. Dar, B. S. Razooky, A. Singh, T. V. Trimeloni, J. M. McCollum, C. D. Cox, M. L. Simpson, L. S. Weinberger, Transcriptional burst frequency and burst size are equally modulated across the human genome. *Proc. Natl. Acad. Sci. U.S.A.* **109**, 17454–17459 (2012).

58. J. J. Gam, B. DiAndreth, R. D. Jones, J. Huh, R. Weiss, A 'poly-transfection' method for rapid, one-pot characterization and optimization of genetic systems. *Nucleic Acids Res.* **47**, e106 (2019).

59. S. Guo, X. Zi, V. P. Schulz, J. Cheng, M. Zhong, S. H. Koochaki, C. M. Megyola, X. Pan, K. Heydari, S. M. Weissman, P. G. Gallagher, D. S. Krause, R. Fan, J. Lu, Nonstochastic reprogramming from a privileged somatic cell state. *Cell* **156**, 649–662 (2014).

60. X. Hu, Q. Wu, J. Zhang, J. Kim, X. Chen, A. A. Hartman, A. E. Eastman, I. H. Park, S. Guo, Reprogramming progressive cells display low CAG promoter activity. *Stem Cells* **39**, 43–54 (2021).

61. Y. S. Michaels, M. B. Barnkob, H. Barbosa, T. A. Baeumler, M. K. Thompson, V. Andre, H. Colin-York, M. Fritzsche, U. Gileadi, H. M. Sheppard, D. J. Knapp, T. A. Milne, V. Cerundolo, T. A. Fulga, Precise tuning of gene expression levels in mammalian cells. *Nat. Commun.* **10**, 818 (2019).

62. A. M. Chiarella, K. V. Butler, B. E. Gryder, D. Lu, T. A. Wang, X. Yu, S. Pomella, J. Khan, J. Jin, N. A. Hathaway, Dose-dependent activation of gene expression is achieved using CRISPR and small molecules that recruit endogenous chromatin machinery. *Nat. Res.* **38**, 50–55 (2020).

63. M. Jost, D. A. Santos, R. A. Saunders, M. A. Horlbeck, J. S. Hawkins, S. M. Scaria, T. M. Norman, J. A. Hussmann, C. R. Liem, C. A. Gross, J. S. Weissman, Titrating gene expression using libraries of systematically attenuated CRISPR guide RNAs. *Nat. Biotechnol.* **38**, 355–364 (2020).

64. R. V. Desai, X. Chen, B. Martin, S. Chaturvedi, D. W. Hwang, W. Li, C. Yu, S. Ding, M. Thomson, R. H. Singer, R. A. Coleman, M. M. Hansen, L. S. Weinberger, A DNA repair pathway can regulate transcriptional noise to promote cell fate transitions. *Science* **373**, eabc6506 (2021).

65. A. Pfeifer, M. Ikawa, Y. Dayn, I. M. Verma, Transgenesis by lentiviral vectors: Lack of gene silencing in mammalian embryonic stem cells and preimplantation embryos. *Proc. Natl. Acad. Sci. U.S.A.* **99**, 2140–2145 (2002).

66. L. Warren, C. Lin, mRNA-based genetic reprogramming. *Mol. Ther.* **27**, 729–734 (2019).

67. J. M. Polo, E. Anderssen, R. M. Walsh, B. A. Schwarz, C. M. Nefzger, S. M. Lim, M. Borkent, E. Apostolou, S. Alaei, J. Cloutier, O. Bar-Nur, S. Cheloufi, M. Stadtfeld, M. E. Figueroa, D. Robinton, S. Natesan, A. Melnick, J. Zhu, S. Ramaswamy, K. Hochedlinger, A molecular roadmap of reprogramming somatic cells into iPS cells. *Cell* **151**, 1617–1632 (2012).

68. N. Maherali, T. Ahfeldt, A. Rigamonti, J. Utikal, C. Cowan, K. Hochedlinger, A high-efficiency system for the generation and study of human induced pluripotent stem cells. *Cell Stem Cell* **3**, 340–345 (2008).

69. A. Somers, J. C. Jean, C. A. Sommer, A. Omari, C. C. Ford, J. A. Mills, L. Ying, A. G. Sommer, J. M. Jean, B. W. Smith, R. Lafyatis, M. F. Demierre, D. J. Weiss, D. L. French, P. Gadue, G. J. Murphy, G. Mostoslavsky, D. N. Kotton, Generation of transgene-free lung disease-specific human induced pluripotent stem cells using a single excisable lentiviral stem cell cassette. *Stem Cells* **28**, 1728–1740 (2010).

70. D. Hockemeyer, F. Soldner, E. G. Cook, Q. Gao, M. Mitalipova, R. Jaenisch, A drug-inducible system for direct reprogramming of human somatic cells to pluripotency. *Cell Stem Cell* **3**, 346–353 (2008).

71. R. Jones, Y. Qian, V. Siciliano, B. DiAndreth, J. Huh, R. Weiss, D. D. Vecchio, An endoribonuclease-based feedforward controller for decoupling resource-limited genetic modules in mammalian cells. *Nat. Commun.* **11**, 5690 (2020).

72. M. Li, J. C. I. Belmonte, Deconstructing the pluripotency gene regulatory network. *Nat. Cell Biol.* **20**, 382–392 (2018).

73. K. Nishimura, T. Kato, C. Chen, L. Oinam, E. Shiomitsu, D. Ayakawa, M. Ohtaka, A. Fukuda, M. Nakanishi, K. Hisatake, Manipulation of KLF4 expression generates iPSCs paused at successive stages of reprogramming. *Stem Cell Rep.* **3**, 915–929 (2014).

74. S. I. Kim, F. Oceguera-Yanez, R. Hirohata, S. Linker, K. Okita, Y. Yamada, T. Yamamoto, S. Yamanaka, K. Woltjen, KLF4 N-terminal variance modulates induced reprogramming to pluripotency. *Stem Cell Rep.* **4**, 727–743 (2015).

75. D. Strebinger, C. Deluz, E. T. Friman, S. Govindan, A. B. Alber, D. M. Suter, Endogenous fluctuations of OCT4 and SOX2 bias pluripotent cell fate decisions. *Mol. Syst. Biol.* **15**, e9002 (2019).

76. Y. Gao, J. Chen, K. Li, T. Wu, B. Huang, W. Liu, X. Kou, Y. Zhang, H. Huang, Y. Jiang, C. Yao, X. Liu, Z. Lu, Z. Xu, L. Kang, J. Chen, H. Wang, T. Cai, S. Gao, Replacement of Oct4 by Tet1 during iPSC induction reveals an important role of DNA methylation and hydroxymethylation in reprogramming. *Cell Stem Cell* **12**, 453–469 (2013).

77. J. Chen, L. Guo, L. Zhang, H. Wu, J. Yang, H. Liu, X. Wang, X. Hu, T. Gu, Z. Zhou, J. Liu, J. Liu, H. Wu, S. Q. Mao, K. Mo, Y. Li, K. Lai, J. Qi, H. Yao, G. Pan, G. L. Xu, D. Pei, Vitamin C modulates TET1 function during somatic cell reprogramming. *Nat. Genet.* **45**, 1504–1509 (2013).

78. J. Shu, C. Wu, Y. Wu, Z. Li, S. Shao, W. Zhao, X. Tang, H. Yang, L. Shen, X. Zuo, W. Yang, Y. Shi, X. Chi, H. Zhang, G. Gao, Y. Shu, K. Yuan, W. He, C. Tang, Y. Zhao, H. Deng, Induction of pluripotency in mouse somatic cells with lineage specifiers. *Cell* **153**, 963–975 (2013).

79. N. Montserrat, E. Nivet, I. Sancho-Martinez, T. Hishida, S. Kumar, L. Miquel, C. Cortina, Y. Hishida, Y. Xia, C. R. Esteban, J. C. I. Belmonte, Reprogramming of human fibroblasts to pluripotency with lineage specifiers. *Cell Stem Cell* **13**, 341–350 (2013).

80. Y. Rais, A. Zviran, S. Geula, O. Gafni, E. Chomsky, S. Viukov, A. A. Mansour, I. Caspi, V. Krupalnik, M. Zerbib, I. Maza, N. Mor, D. Baran, L. Weinberger, D. A. Jaitin, D. Lara-Astiaso, R. Blecher-Gonen, Z. Shipony, Z. Mukamel, T. Hagai, S. Gilad, D. Amann-Zalcenstein, A. Tanay, I. Amit, N. Novershtern, J. H. Hanna, Deterministic direct reprogramming of somatic cells to pluripotency. *Nature* **502**, 65–70 (2013).

81. P. W. Hill, R. Amouroux, P. Hajkova, DNA demethylation, Tet proteins and 5-hydroxymethylcytosine in epigenetic reprogramming: An emerging complex story. **104**, 324–333 (2014).

82. T. A. Hore, F. V. Meyenn, M. Ravichandran, M. Bachman, G. Ficz, D. Oxley, F. Santos, S. Balasubramanian, T. P. Jurkowski, W. Reik, Retinol and ascorbate drive erasure of epigenetic memory and enhance reprogramming to naïve pluripotency by complementary mechanisms. *Proc. Natl. Acad. Sci. U.S.A.* **113**, 12202–12207 (2016).

83. S. Jaffer, P. Goh, M. Abbasian, A. C. Nathwani, Mbd3 promotes reprogramming of primary human fibroblasts. *Int. J. Stem Cells* **11**, 235–241 (2018).

84. K. Adachi, W. Kopp, G. Wu, S. Heising, B. Greber, M. Stehling, M. J. Araúzo-Bravo, S. T. Boerno, B. Timmermann, M. Vingron, H. R. Schöler, Esrrb unlocks silenced enhancers for reprogramming to naive pluripotency. *Cell Stem Cell* **23**, 266–275.e6 (2018).

85. N. Mor, Y. Rais, D. Sheban, S. Peles, A. Aguilera-Castrejon, A. Zviran, D. Elinger, S. Viukov, S. Geula, V. Krupalnik, M. Zerbib, E. Chomsky, L. Lasman, T. Shani, J. Bayerl, O. Gafni, S. Hanna, J. D. Buenrostro, T. Hagai, H. Masika, G. Vainorius, Y. Bergman, W. J. Greenleaf, M. A. Esteban, U. Elling, Y. Levin, R. Massarwa, Y. Merbl, N. Novershtern, J. H. Hanna, Neutralizing Gatad2a-Chd4-Mbd3/NuRD complex facilitates deterministic induction of naive pluripotency. *Cell Stem Cell* **23**, 412–425.e10 (2018).

86. G. J. Markov, T. Mai, S. Nair, A. Shcherbina, Y. X. Wang, D. M. Burns, A. Kundaje, H. M. Blau, Ap-1 is a temporally regulated dual gatekeeper of reprogramming to pluripotency. *Proc. Natl. Acad. Sci. U.S.A.* **118**, e2104841118 (2021).

87. H. Park, B. Cho, J. Kim, Rad50 mediates DNA demethylation to establish pluripotent reprogramming. *Exp. Mol. Med.* **52**, 1116–1127 (2020).

88. R. Navarro, L. C. Chen, R. Rakhit, T. J. Wandless, A novel destabilizing domain based on a small-molecule dependent fluorophore. *ACS Chem. Biol.* **11**, 2101–2104 (2016).

89. Y. Miyazaki, H. Imoto, L. C. Chen, T. J. Wandless, Destabilizing domains derived from the human estrogen receptor. *J. Am. Chem. Soc.* **134**, 3942–3945 (2012).

90. J. A. Casas-Mollano, M. H. Zinselmeier, S. E. Erickson, M. J. Smanski, CRISPR-Cas activators for engineering gene expression in higher eukaryotes. *CRISPR J.* **3**, 350–364 (2020).

91. R. Morita, M. Suzuki, H. Kasahara, N. Shimizu, T. Shichita, T. Sekiya, A. Kimura, K. I. Sasaki, H. Yasukawa, A. Yoshimura. ETS transcription factor ETV2 directly converts human fibroblasts into functional endothelial cells. *Proc. Natl. Acad. Sci. U.S.A.* **112**, 160–165 (2015).

92. H. Xie, M. Ye, R. Feng, T. Graf. Stepwise reprogramming of B cells into macrophages, *Cell* **117**, 663–676 (2004).

93. L. Warren, P. D. Manos, T. Ahfeldt, Y. H. Loh, H. Li, F. Lau, W. Ebina, P. K. Mandal, Z. D. Smith, A. Meissner, G. Q. Daley, A. S. Brack, J. J. Collins, C. Cowan, T. M. Schlaeger, D. J. Rossi, Highly efficient reprogramming to pluripotency and directed differentiation of human cells with synthetic modified mRNA. *Cell Stem Cell* **7**, 618–630 (2010).

94. S. Liedtke, J. Enczmann, S. Waclawczyk, P. Wernet, G. Kögler, Oct4 and its pseudogenes confuse stem cell research. *Cell Stem Cell* **1**, 364–366 (2007).

95. Z. Redshaw, A. J. Strain, Human haematopoietic stem cells express Oct4 pseudogenes and lack the ability to initiate Oct4 promoter-driven gene expression. *J. Negat. Results Biomed.* **9**, 2 (2010).

96. X. Duportet, L. Wroblewska, P. Guye, Y. Li, J. Eyquem, J. Rieders, T. Rimchala, G. Batt, R. Weiss, A platform for rapid prototyping of synthetic gene networks in mammalian cells. *Nucleic Acids Res.* **42**, 13440–13451 (2014).

97. N. W. Meza, A. Puyet, S. Pérez-Benavente, O. Quintana-Bustamante, A. Diez, J. A. Bueren, J. C. Segovia, J. M. Bautista, Functional analysis of gammaretroviral vector transduction by quantitative PCR. *J. Gene Med.* **8**, 1097–1104 (2006).

98. B. Fehse, O. S. Kustikova, M. Bubenheim, C. Baum, Pois(s)on—It's a question of dose. *Gene Ther.* **11**, 879–881 (2004).

99. S. Charrier, M. Ferrand, M. Zerbato, G. Précigout, A. Viornery, S. Bucher-Laurent, S. Benkhelifa-Ziyyat, O. W. Merten, J. Perea, A. Galy, Quantification of lentiviral vector copy numbers in individual

hematopoietic colony-forming cells shows vector dose-dependent effects on the frequency and level of transduction. *Gene Ther.* **18**, 479–487 (2011).

100. J. R. Lin, M. Fallahi-Sichani, P. K. Sorger, Highly multiplexed imaging of single cells using a high-throughput cyclic immunofluorescence method. *Nat. Commun.* **6**, 8390 (2015).

101. A. Gerrits, B. Dykstra, O. J. Kalmykowa, K. Klauke, E. Verovskaya, M. J. Broekhuis, G. De Haan, L. V. Bystrykh, Cellular barcoding tool for clonal analysis in the hematopoietic system. *Blood* **115**, 2610–2618 (2010).

102. D. T. Gillespie, Exact stochastic simulation of coupled chemical reactions. *J. Phys. Chem.* **81**, 2340–2361 (1977).

103. N. Zapata-Linares, S. Rodriguez, E. Salido, G. Abizanda, E. Iglesias, F. Prosper, G. Gonzalez-Aseguinolaza, J. R. Rodriguez-Madoz, Generation and characterization of human iPSC lines derived from a Primary Hyperoxaluria Type I patient with p.I244T mutation. *Stem Cell Res.* **16**, 116–119 (2016).

104. N. T. Swaidan, S. Salloum-Asfar, F. Palangi, K. Errafii, N. H. Soliman, A. T. Aboughalia, A. H. S. Wali, S. A. Abdulla, M. M. Emara, Identification of potential transcription factors that enhance human iPSC generation. *Sci. Rep.* **10**, 21950 (2020).